Fabrication and field-emission performance of zirconium disulfide nanobelt arrays

Yu-Ling Zhang, Xing-Cai Wu,* You-Rong Tao, Chang-Jie Mao and Jun-Jie Zhu

Received (in Cambridge, UK) 17th March 2008, Accepted 2nd May 2008
First published as an Advance Article on the web 14th May 2008
DOI: 10.1039/b804528c

Crystal ZrS_2 nanobelt quasi-arrays were fabricated by pyrolysis of the ZrS_3 nanobelt quasi-arrays in vacuum; field-emission measurements show that the ZrS_2 nanobelt arrays are decent field emitters with a turn-on field of $\sim$0.95 V μm^{-1} and a threshold field of 3.6 V μm^{-1}.

Over the past decade considerable attention has been paid to the preparation and the properties of one-dimensional (1D) nanostructures because of their distinctive geometries, unique physical properties originating from a quantum-confinement effect, and potential application in nanodevices.[1–5] Field emission (FE) is based on the physical phenomenon of quantum tunneling, during which electrons are injected from a material surface into vacuum under the influence of an applied electric field.[6] Research shows that aligned 1D nanostructures with a high packing density can significantly enhance the material FE properties,[7] therefore many field emitters were fabricated into 1D nanostructured arrays such as carbon nanotubes,[8] SiC nanocones,[9] and Mo nanowires.[10]

Zirconium disulfide (ZrS_2) is an important semiconductor with a wide bandgap energy of 1.4 eV,[11] and possesses good conductivity. Its crystal contains a metal layer sandwiched between two chalcogen layers with the metal in an octahedral coordination mode.[12] Nanotubes and nanowires of ZrS_2 have been prepared,[13,14] but all of the reported ZrS_2 nanostructures were distributed randomly in powder form. Herein, we describe a new strategy for the fabrication of quasi-aligned ZrS_2 nanobelt arrays by a two-step method: firstly the ZrS_3 nanobelt arrays were grown on Zr foils through a chemical-vapor-transport (CVT) approach of sulfur, then the ZrS_3 nanobelt arrays were thermolyzed to ZrS_2 nanobelt arrays in vacuum.† FE characteristics of the arrays were analyzed. The arrays displayed a low turn-on field of $\sim$0.95 V μm^{-1} and a field-enhancement factor of 2.5×10^4. To our knowledge, the preparation and field-emission performance of ZrS_2 nanobelt arrays have not been reported to date.

The structure of the products was examined using a Shimadzu XRD-6000 X-ray diffractometer (XRD) with graphite monochromatized Cu Kα-radiation and a JEOL Model JEM-2100 high-resolution electron microscope (HRTEM). The morphologies were characterized by a JEOL-JEM 200CX transmission electron microscope (TEM) with a selected area electron diffraction (SAED) attachment, and a LEO-1530VP scanning electron microscope (SEM) with energy-dispersive X-ray spectrometer (EDX). The electron field-emission measurements were performed by using a parallel-plate configuration with a space of 225 μm in a vacuum chamber at a pressure of 5.0×10^{-4} Pa at room temperature. A dc voltage sweeping from 0 to 2090 V was applied to the sample.

Fig. 1(a) and (b) show XRD patterns of monoclinic ZrS_3 (JCPDS File 30-1498) and hexagonal ZrS_2 (JCPDS File 11-0679) nanobelt arrays, respectively. Impure peaks originate from the Zr substrate. Fig. 2(a) and (b) display SEM images of the ZrS_3 nanobelt arrays grown on the Zr foil. Typical ZrS_3 nanobelts have a rectangular section of $\sim 85 \times 480$ nm^2. On the basis of the SEM observations, the nanobelts have a thickness of about 45–120 nm, a width of about 200–2000 nm, and a length of about 5–70 μm. Fig. 2(c) reveals a TEM image and SAED pattern of a single nanobelt with a width of about 600 nm. The SAED pattern (inset in Fig. 2c) supports the result of the above XRD, and reveals that the nanobelt grew along the [010] direction. Fig. 2(d) shows a HRTEM image and corresponding Fourier transform (inset) of a single

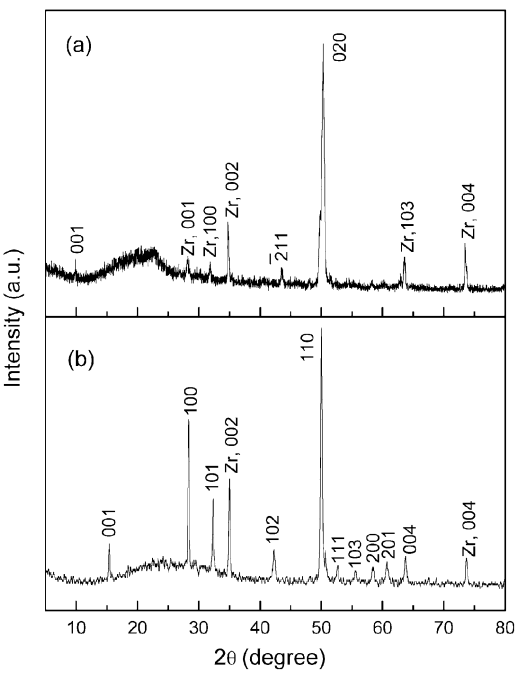

Fig. 1 Powder XRD patterns of (a) ZrS_3 nanobelts and (b) ZrS_2 nanobelts. Impure peaks can be attributed to Zr.

Key Laboratory of Mesoscopic Chemistry of MOE, State Key Laboratory of Coordination Chemistry, and School of Chemistry and Chemical Engineering, Nanjing University, Nanjing 210093, China. E-mail: wuxingca@netra.nju.edu.cn; Fax: +86-25-83317761; Tel: +86-25-83597374

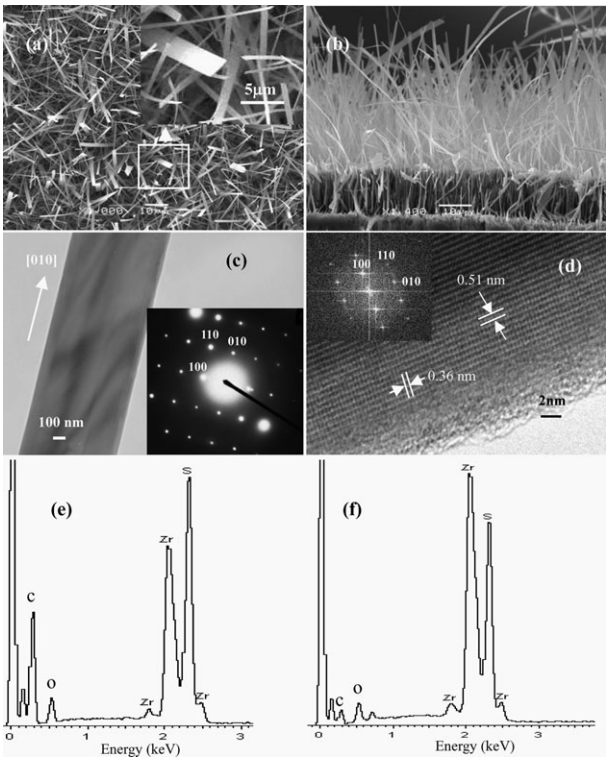

Fig. 2 (a, b) SEM images of ZrS_3 nanobelt arrays (inset in Fig. 2a shows a magnified image of the white box in Fig. 2a). (c) TEM image and SAED pattern (inset) of a single ZrS_3 nanobelt. (d) HRTEM image and corresponding Fourier transform (inset) of a single ZrS_3 nanobelt. (e) EDX spectrum of a single ZrS_3 nanobelt. (f) EDX spectrum of a single ZrS_2 nanobelt.

ZrS_3 nanobelt. Fringe spacings of 0.51 and 0.36 nm correspond to spaces of (010) and (100) planes of monoclinic ZrS_3 (JCPDS File 30-1498), respectively, which further confirms that the nanobelt grew along the [010] direction. The EDX analysis for a single nanobelt (Fig. 2e) shows that the atomic ratio of zirconium and sulfur is 26.3 : 73.7 (1 : 2.8), which is in approximate agreement with the ratio of ZrS_3. Carbon and oxygen peaks arise from adhesive from the sample desk.

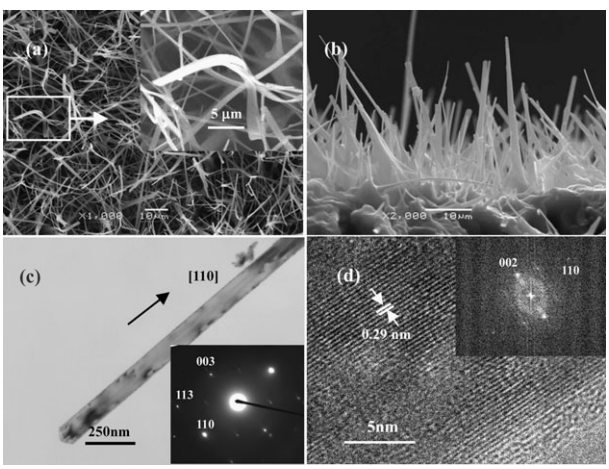

Fig. 3 (a, b) SEM images of the ZrS_2 nanobelt arrays (inset in Fig. 3a shows a magnified image of the white box in Fig. 3a). (c) TEM image and SAED pattern (inset) of a single ZrS_2 nanobelt. (d) HRTEM image and corresponding Fourier transform (inset) of a single ZrS_2 nanobelt.

Fig. 3(a) and (b) show SEM images of the ZrS_2 nanobelt arrays converted from the above ZrS_3 nanobelts. They reveal that the belt-like morphology was still kept after the ZrS_3 nanobelts were pyrolyzed to ZrS_2 phase in vacuum, and the size of the ZrS_2 nanobelts approaches that of the original ZrS_3 nanobelt templates. For example, a typical ZrS_2 nanobelt has a rectangular section of $\sim 80 \times 480$ nm^2. Fig. 3(c) shows a TEM image and SAED pattern (inset) of an individual ZrS_2 nanobelt; the nanobelt has a tip end. The SAED pattern further confirms that the nanobelt is ZrS_2 nanobelt (JCPDS File 11-0679), and grew along the [110] direction. Fig. 3(d) displays a HRTEM image and corresponding Fourier transform (inset) of a single ZrS_2 nanobelt. Fringe spacings of 0.29 nm correspond to the space of the (002) plane of hexagonal ZrS_2 (JCPDS File 11-0679). The Fourier transform electronic diffraction pattern (inset in Fig. 3d) still shows the growth of the ZrS_2 along the [110] direction. The EDX analysis for a single ZrS_2 nanobelt (Fig. 2f) shows that the atomic ratio of zirconium and sulfur is 36.0 : 64.0 (1 : 1.8), which is in approximate agreement with the ratio of ZrS_2. Similarly, carbon and oxygen peaks arise from adhesive from the sample desk.

Based on the above observations, a modified vapor–solid (VS) mechanism may account for the formation of the ZrS_3 nanobelt. As the reaction temperature gradually increased to 650 °C, sulfur (bp 444.6 °C) was evaporated into gas form, and deposited on the Zr substrate. Then zirconium reacted with sulfur vapors, and formed unstable ZrS_x in the gas phase. ZrS_x in the vapor phase reacted with S vapor, and condensed again on the Zr substrate to form stable ZrS_2 seeds. In the following process, ZrS_x and S in the vapor phase might have combined with ZrS_2 seeds to form ZrS_3 nanobelts due to the inducement of the seeds. Then the ZrS_3 nanobelts were thermolyzed to ZrS_2 nanobelts in vacuum.

Fig. 4 exhibits a curve of current density *versus* applied field of the ZrS_2 nanobelt arrays. From the curve, a turn-on field of ~ 0.95 V μm^{-1} (defined as the applied field for 10 μA cm^{-2}) and a threshold field of ~ 3.6 V μm^{-1} (defined as the applied field for 1 mA cm^{-2}) were obtained. The turn-on field of the ZrS_2 nanobelt arrays is lower than those reported for Mo nanowires (2.2 V μm^{-1}),[10] AlN nanorods (3.8 V μm^{-1}),[15] TaS_2 nanobelts (19.8 V μm^{-1}),[16] and Si cones (13–16.5 V μm^{-1}),[17] so the ZrS_2 nanobelt arrays are excellent electronic field

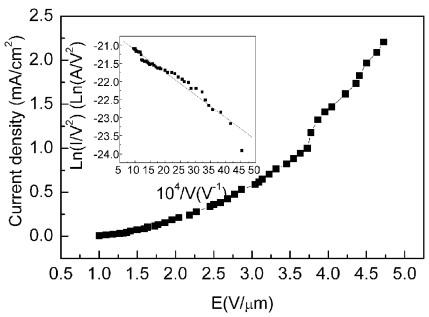

Fig. 4 Current density–electric field curve of ZrS_2 nanobelt arrays. The inset is the corresponding F–N plot.

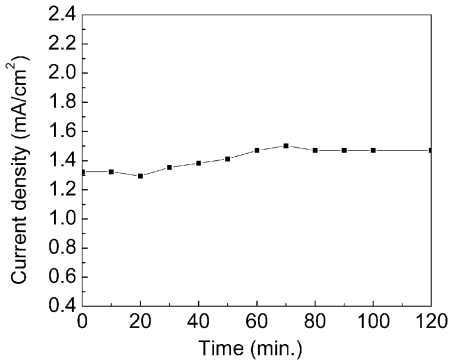

Fig. 5 A current density–time plot of quasi-aligned ZrS_2 nanobelt arrays at an applied electric field of 3.86 V μm^{-1}.

emitters. The emission current–voltage characteristics were analyzed by using the Fowler–Nordheim (F–N) equation for the field emission:[18] $J = A(\beta^2V^2d^{-2}/\Phi)\exp(-B\Phi^{3/2}\beta^{-1}d/V)$, where J ($= I/\alpha$) is the current density (A m^{-2}), $A = 1.56 \times 10^{-10}$ (A V^{-2} eV), $B = 6.83 \times 10^9$ ($eV^{-3/2}$ V m^{-1}), α is the effective emission area, I is the current intensity (A), d is a distance between the anode and the cathode, V is the applied voltage, β is a field enhancement factor, and Φ is the work function for the emitting materials, which is 4.95 eV for ZrS_2.[19] By plotting ln (I/V^2) *versus* $1/V$, the F–N curve of the ZrS_2 nanobelt arrays was obtained (inset in Fig. 4).

From the slope of the F–N curve, a field enhancement factor β of $\sim 2.5 \times 10^4$ was calculated for the ZrS_2 nanobelt. The linearity of the curves implies that the field emissions from the nanobelts follow FN theory and the emitted current is indeed caused by quantum tunneling.[20] In addition, the emission current density of the ZrS_2 nanobelt arrays was measured within 2 h at an applied electric field of 3.86 V μm^{-1}. The initial current density and the average current densities are 1.32 and 1.28 mA cm^{-2}, respectively. No notable current density degradation was observed, and the emission current fluctuations were as low as 3.13%, proving the high stability of ZrS_2 aligned emitters (Fig. 5).

In summary, we have demonstrated an effective approach for the synthesis of single-crystalline ZrS_2 nanobelt quasi-arrays. The aligned arrays possess a low turn-on field of ~ 0.95 V μm^{-1} and a high field enhancement factor β of $\sim 2.5 \times 10^4$. They also reveal an emission current density of ~ 2.2 mA cm^{-2} at a microscopic field of 4.7 V μm^{-1}. The arrays display good stability of the field emission. These properties make the nanobelt arrays ensemble highly valuable for novel FE nanodevices. Because ZrS_2 with a layer structure can be intercalated by Li^+, the nanostructures may find an application in lithium batteries as anode material, and can even be used for rechargeable lithium batteries to yield specific capacity.

The work was financially supported by the National Science Foundations of China (No. 20671050) and the National Basic Research Program of China (973 Program, No.2007CB936302).

Notes and references

† In a typical procedure, zirconium foils (99.8%; thickness: 0.2 mm) and sulfur powders (99.8%) were used. The procedure was divided into two steps. Firstly, Zr foil (83.6 mg) and S powders (88.5 mg) were sealed in a quartz ampoule under vacuum (Φ 6 mm $\times$ 10 mm, *ca.* 10^{-2} Pa). Then the ampoule was placed in a conventional horizontal furnace (temperature gradient: *ca.* 10 K cm^{-1}, furnace tube: Φ 5 cm $\times$ 30 cm), and the end with Zr foils was put at the center of the furnace. After the furnace was maintained at 650 °C for 5 h, large-scale ZrS_3 nanobelt arrays grew on the Zr foils. The furnace was cooled to room temperature, then the foils with the ZrS_3 nanobelts were extracted from the quartz ampoule, and again sealed in another quartz ampoule under vacuum (Φ 6 mm $\times$ 26 mm, *ca.* 10^{-2} Pa). Then one end of the quartz ampoule with the ZrS_3 nanobelt arrays was again placed at the center of the horizontal furnace, and remained at 820 °C for 1.5 h in the flowing argon atmosphere while the other end was extended about 10 cm outside of the furnace so that the thermolyzed sulfur was deposited on the cool end. After the reaction had finished and the ampoule had cooled to room temperature, the foils with ZrS_2 nanobelt arrays were extracted from the ampoule.

1 M. G. Bawendi, M. L. Steigerwald and L. E. Brus, *Annu. Rev. Phys. Chem.*, 1990, **41**, 477.
2 A. P. Alivisatos, *Science*, 1996, **271**, 933.
3 H. Weller, *Angew. Chem., Int. Ed. Engl.*, 1993, **32**, 41.
4 X. Duan, Y. Huang, Y. Cui, J. Wang and C. M. Lieber, *Nature*, 2001, **409**, 66.
5 N. I. Konvtyukhova and T. E. Mallouk, *Chem.–Eur. J.*, 2002, **32**, 435.
6 N. S. Xu and S. E. Huq, *Mater. Sci. Eng., R*, 2005, **48**, 47.
7 W. Z. Wang, B. Q. Zeng, J. Yang, B. Poudel, J. Y. Huang, M. J. Naughton and Z. F. Ren, *Adv. Mater.*, 2006, **18**, 3275.
8 H. Araki, T. Katayama and K. Yoshino, *Appl. Phys. Lett.*, 2001, **79**, 2636.
9 Z. S. Wu, S. Z. Deng, N. S. Xu, J. Chen and J. Zhou, *Appl. Phys. Lett.*, 2002, **80**, 3829.
10 J. Zhou, N. S. Xu, S. Z. Deng, J. Chen, J. C. She and Z. L. Wang, *Adv. Mater.*, 2003, **15**, 1835.
11 A. H. Reshak and S. Auluck, *Physica B*, 2004, **353**, 230.
12 L. F. Mattesiss, *Phys. Rev. B: Solid State*, 1973, **8**, 3719.
13 M. Nath and C. N. R. Rao, *Angew. Chem., Int. Ed.*, 2002, **41**, 3451.
14 T. Liu, J. Yu and M. Chen, *Ceram. Int.*, 2007, **33**, 321.
15 J. H. He, R. Yang, Y. L. Chueh, L. J. Chou, L. J. Chen and Z. L. Wang, *Adv. Mater.*, 2006, **18**, 650.
16 X. C. Wu, Y. R. Tao, Y. M. Hu, Y. Song, Z. Hu, J. J. Zhu and L. Dong, *Nanotechnology*, 2006, **17**, 201.
17 N. G. Shang, F. Y. Meng, F. C. K. Au, Q. Li, C. S. Lee, I. Bello and S. T. Lee, *Adv. Mater.*, 2002, **14**, 1308.
18 R. H. Fowler and L. W. Nordheim, *Proc. R. Soc. London, Ser. A*, 1928, **119**, 173.
19 R. B. Murray and R. H. Williams, *Philos. Mag.*, 1974, **29**(3), 473.
20 C. T. Hsieha, J. M. Chen, H. H. Lin and H. C. Shih, *Appl. Phys. Lett.*, 2003, **83**, 3383.